RSC Advances

PAPER

View Article Online
View Journal | View Issue



Cite this: *RSC Adv.*, 2024, **14**, 37628

# Magnetoresistance effect of nitrogen doped graphdiyne†

Huifang Kang,[a] Yi Zhong,[b] Peiyan Gao,[b] Xiong Liang,[a] Huiye Qiu*[a] and Yongping Zheng*[b]

This investigation elucidates the influence of nitrogen doping (N-doping) on the magnetoresistance (MR) characteristics of graphdiyne (GDY) by methodically adjusting the levels of N-doping. Through exhaustive experimental analyses, encompassing SEM, XPS, and magneto-transport measurements, we demonstrate that N-doping markedly augments carrier concentration, thereby inducing distinct MR behaviors. Specifically, $N_{30}$-GDY manifests negative magnetoresistance (NMR) attributable to weak localization phenomena, whereas $N_{60}$-GDY and $N_{90}$-GDY exhibit positive magnetoresistance (PMR) characterized by significant resistance enhancements. These results not only clarify the underlying mechanisms governing the MR properties of GDY but also introduce a novel strategy for optimizing MR performance *via* controlled heteroatom doping, thereby holding considerable implications for the advancement of carbon-based electronic devices.

Received 17th October 2024
Accepted 18th November 2024

DOI: 10.1039/d4ra07434c

rsc.li/rsc-advances



## Introduction

In 2010, the synthesis of a novel two-dimensional (2D) carbon material, graphdiyne (GDY), was successfully achieved through a crosslinking reaction.[1] Comprising sp- and $sp^2$-hybridized carbon atoms, GDY has attracted considerable attention owing to its remarkable properties.[2–6] As an allotrope of graphene with a direct bandgap structure proximate to the Dirac cone, theoretical predictions estimate GDY's bandgap to range from 0.46 to 1.22 eV,[7,8] with carrier mobility comparable to that of graphene.[9] Its unique structural configuration and acetylenic bonds render GDY highly conducive to carrier transport, attaining mobilities as high as $10^4$ to $10^5$ $cm^2$ $V^{-1}$ $s^{-1}$,[10] thereby indicating substantial potential for applications in carbon-based electronic devices.

In recent years, GDY has been extensively investigated in domains such as energy,[11] catalysis,[12] and magnetism,[13] however, its magnetoresistance (MR) properties remain largely unexplored. Although several studies have examined the MR characteristics of GDY, the complex factors influencing its MR behavior are still inadequately understood and insufficiently explored. Among the myriad factors affecting GDY's MR properties, carrier concentration emerges as a pivotal parameter. According to the literature, nitrogen doping (N-GDY) has been demonstrated as an effective method for enhancing carrier concentration.[14] Nitrogen doping introduces novel electronic states and disrupts the symmetry of the GDY lattice, thereby modulating its electronic, magnetic, and optical properties. Due to the analogous atomic sizes of nitrogen and carbon, nitrogen can be seamlessly integrated into the GDY lattice, resulting in stable nitrogen-doped GDY structures. This incorporation significantly alters the electronic band structure of GDY, facilitating tunable magnetoresistance. Empirical evidence has corroborated that nitrogen doping effectively increases carrier concentration.[14] Consequently, nitrogen doping presents a promising strategy for further manipulating the MR properties of GDY.

In this study, we fabricated nitrogen-doped GDY samples with varying nitrogen content, resulting in significant modifications to their MR properties. Specifically, under an applied magnetic field of 9 tesla (T) and at a temperature of 2 kelvin (K), $N_{30}$-GDY exhibited negative magnetoresistance (NMR) with a maximum MR of 200%, indicative of weak localization effects. In contrast, $N_{60}$-GDY and $N_{90}$-GDY demonstrated positive magnetoresistance (PMR) characterized by pronounced resistance enhancements, with $N_{60}$-GDY exhibiting a particularly robust PMR effect, exceeding a 400% resistance change. At lower levels of nitrogen doping, the increased carrier concentration enhances electron scattering in the magnetic field, thereby augmenting MR. These distinct magnetoresistance behaviors in nitrogen-doped GDY suggest a substantial transformation in its transport properties resulting from nitrogen incorporation.

### Experiment

**Synthesis of GDY.** In this study, GDY was synthesized employing a cross-coupling methodology based on previously

[a]*School of Physics and Mechanical and Electronical Engineering, Longyan University, Longyan 364012, China*

[b]*College of Physics and Energy, Fujian Normal University, Fujian Provincial Key Laboratory of Quantum Manipulation and New Energy Materials, Fuzhou, 350117, China. E-mail: zyp@fjnu.edu.cn*

† Electronic supplementary information (ESI) available. See DOI: https://doi.org/10.1039/d4ra07434c

established protocols.[1] We replaced the copper substrate, which was required for the experiment, with $Si/SiO_2/Cu$, using it as the growth substrate for GDY.[15] The experimental procedure commenced with the deposition of a nanoscale copper (Cu) layer onto a $Si/SiO_2$ substrate *via* magnetron sputtering, thereby establishing the requisite $Si/SiO_2/Cu$ foundation for GDY synthesis. The Cu layer functions dually as a substrate for GDY growth and as an active catalyst during synthesis. The $Si/SiO_2/Cu$ substrate was introduced into a three-necked flask containing 50 mL of pyridine. Concurrently, trimethylsilyl ethynyl benzene dissolved in tetrahydrofuran, along with tetrabutylammonium fluoride, was reacted under low-temperature, argon-protected conditions for 15 minutes until the emergence of a purple-red hue signified the reaction's completion. The resultant solution was subsequently processed to obtain HEB powder through dilution with ethyl acetate, washing with sodium chloride, and drying over anhydrous sodium sulfate. Subsequently, 40 mL of pyridine was added to the HEB powder, which was then slowly transferred to the flask containing the $Si/SiO_2/Cu$ substrate over an 8 hours period to ensure uniform dispersion. The reaction system was maintained under argon protection in the dark for three days, facilitating the formation of GDY films on the Cu-coated substrate.

**Synthesis of N-GDY.** The GDY film specimens were positioned within a tubular furnace, where a continuous flow of $NH_3$ gas was introduced to sustain the furnace environment. Upon reaching a temperature of 550 °C, the furnace temperature was stabilized for durations of 30, 60, and 90 minutes, respectively. Following each isothermal treatment and subsequent cooling to ambient temperature, the $NH_3$ gas supply was terminated, culminating in the synthesis of N-GDY films. The samples subjected to constant temperatures for 30, 60, and 90 minutes were designated as $N_{30}$-GDY, $N_{60}$-GDY, and $N_{90}$-GDY, respectively (Fig. 1).

The morphologies of the samples were scrutinized using a scanning electron microscope (SEM, JSM-7500 F, Japan). Raman spectra were obtained with a LABRAM-HR micro-Raman system (Longjumeau, Paris, France). The chemical compositions of the samples were analyzed *via* X-ray photoelectron spectroscopy (XPS, ESCALAB 250, VG, USA). The thicknesses of the GDY films were measured using atomic force microscopy (Bruker Dimension ICON, Germany).

Four-probe magneto-transport measurements were executed utilizing a physical property measurement system (PPMS, Quantum Design, Dynacool D204, USA) over a temperature range of 2 to 150 K and within magnetic fields up to 9 T. Resistances were gauged by applying a fixed electric current of 0.03 mA, with the magnetic field ($B$) oriented along the vertical axis, perpendicular to the direction of the electric current. Hall resistivity measurements were conducted under a fixed electric current of 0.038 mA. Electron paramagnetic resonance (EPR) spectra were recorded using an X-band (9.6 GHz) Bruker EMX-nano spectrometer at room temperature, with the magnetic field oriented perpendicular to the substrate (approximately 0.335 T).

## Result and discuss

SEM analysis (as illustrated in Fig. 2) was performed to examine the samples with varying nitrogen levels ($N_{30}$-GDY, $N_{60}$-GDY, and $N_{90}$-GDY). The results indicate that all GDY films, irrespective of nitrogen content, exhibit exceptional uniformity and continuity. Notably, the morphology and structural integrity of the films remain virtually unaltered despite variations in N-doping levels. The SEM images display smooth, planar surfaces with minimal disruptions to the GDY films. Furthermore, cross-sectional SEM images reveal consistent features across all samples, including a uniform thickness of approximately 50 nanometers and distinct interlayer boundaries. These structural characteristics establish a robust foundation for subsequent MR investigations.

The structural characteristics of GDY and N-GDY films, grown directly on the substrate, were characterized using Raman spectroscopy. As depicted in Fig. 3 and S1,† four primary peaks are discernible: the D peak at 1358.9 $cm^{-1}$, the G peak at 1598.1 $cm^{-1}$, and two weaker peaks corresponding to the –C≡C– acetylene bonds. The D peak, situated at 1358.9 $cm^{-1}$, signifies the presence of defects within the sample, with findings suggesting a substantial increase in defect density post N-doping.[16] The G peak, at 1598.1 $cm^{-1}$, is attributed to first-order scattering and the breathing vibrations of the $E_{2g}$ modes within the $sp^2$-hybridized carbon domains of the aromatic ring, characterized by in-phase stretching vibrations.[17] The morphology

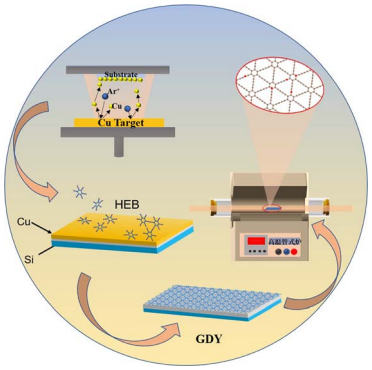


Fig. 1 Schematic diagram for the synthesis of N-GDY.

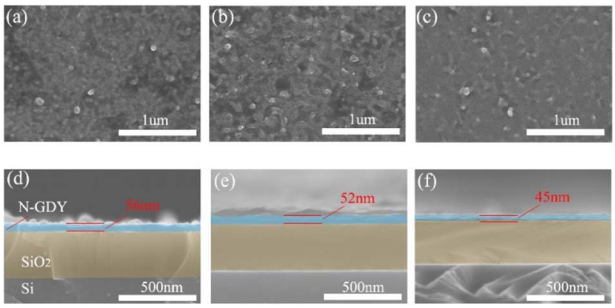


Fig. 2 (a–c) Exhibit the SEM morphologies of $N_{30}$-GDY, $N_{60}$-GDY, and $N_{90}$-GDY samples, respectively. (d–f) Exhibit the cross-sectional SEM morphologies of $N_{30}$-GDY, $N_{60}$-GDY, and $N_{90}$-GDY samples, respectively.

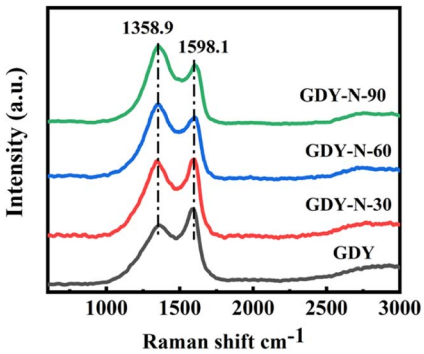


Fig. 3 Raman spectra of $N_{30}$-GDY, $N_{60}$-GDY and $N_{90}$-GDY.

of this peak corroborates the conclusion that the $I_D/I_G$ ratio, derived from the spectrum, escalates with prolonged annealing durations (30, 60, 90 minutes). This implies a proliferation of defects in GDY correlating with increased $NH_3$ annealing time.

Subsequent XPS analysis was undertaken to further elucidate the chemical structure of N-doped GDY samples. As presented in Fig. 4 and S2,† the comprehensive XPS spectrum confirms that GDY comprises exclusively carbon (C) and oxygen (O). Moreover, with extended $NH_3$ annealing times, the intensity of the nitrogen (N) peak intensifies, unequivocally confirming the successful incorporation of nitrogen into the GDY films. The peak at 284.8 eV corresponds to the C 1s orbital. Due to GDY's exposure to ambient air, an O 1s signal, attributed to adsorbed $O_2$, is detected at 531.6 eV.[18,19] Following $NH_3$ treatment at 550 °C, N-GDY was formed, and its N 1s peak was observed at 398.6 eV. The C 1s peak of GDY can be deconvoluted into four components: C–C ($sp^2$) at 284.4 eV, C=C (sp) at 285.0 eV, C–O at 285.6 eV, and C=O at 287.7 eV. In contrast, N-GDY exhibits peaks at 284.4 eV, 285.0 eV, 285.6 eV, 286.4 eV, and 287.9 eV, corresponding to C–C ($sp^2$), C=C (sp), C–O, C=N, and C=O

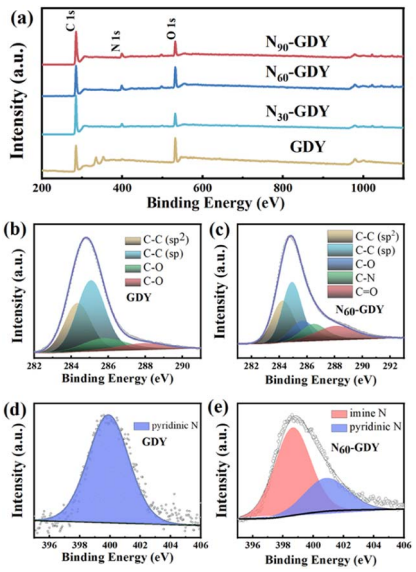


Fig. 4 (a) XPS spectra (survey) of $N_{30}$-GDY, $N_{60}$-GDY and $N_{90}$-GDY. (b) and (c) are XPS C 1s spectra of GDY and $N_{60}$-GDY, respectively. (d) and (e) is the XPS N 1s spectrum of GDY and $N_{60}$-GDY, respectively.

bonds, respectively.[16,20,21] The N 1s peak can be further deconvoluted into two distinct peaks at 398.5 eV and 399.9 eV (as depicted in Fig. 4). The peak at 398.5 eV is ascribed to nitrogen derived from $NH_3$, whereas the peak at 399.9 eV corresponds to pyridinic nitrogen.[20,22,23]

Electron paramagnetic resonance (EPR) measurements were conducted at ambient temperature to assess the spin concentration and *g*-factor of the material. As illustrated in Fig. S3,† the spin concentration ($N_S$), directly correlated with the intensity of the EPR peak, was quantified. The spin concentrations for $N_{30}$-GDY, $N_{60}$-GDY, and $N_{90}$-GDY were determined to be $2.34 \times 10^{11}$ spins per $mm^3$, $7.76 \times 10^{11}$ spins per $mm^3$, and $16.29 \times 10^{11}$ spins per $mm^3$, respectively. The experimental *g*-factors were recorded as 2.0050, 2.0049, and 2.0053 for $N_{30}$-GDY, $N_{60}$-GDY, and $N_{90}$-GDY, respectively. This suggests the presence of nitrogen-related vacancies or defects within the sample, thereby further corroborating the successful doping of nitrogen into the GDY structure.[24] Notably, the EPR peak intensity escalates with increasing nitrogen concentrations, indicating that spin–orbit coupling and electron–nuclear interactions remain minimal in typical organic aromatic systems, thereby providing clear evidence for the existence of free radicals.

The transport properties of $N_{30}$-GDY, $N_{60}$-GDY, and $N_{90}$-GDY samples were scrutinized by analyzing their resistivity variations with temperature (ranging from 2 to 120 K) under zero-field conditions. As depicted in Fig. S4,† the resistivity curve exhibits a distinct inflection point, signifying a transition from metallic behavior at low temperatures (2–18 K) to semiconducting characteristics at elevated temperatures (18–100 K). Additionally, Fig. S5† underscores our utilization of density functional theory (DFT) to compute the band gap of N-doped GDY, revealing that N-doping effectively diminishes the band gap, thereby endowing the material with metallic properties.

Further analysis of carrier dynamics in GDY post N-doping was conducted through Hall resistivity measurements. Notably, Fig. S6† illustrates a nonlinear correlation between Hall resistivity and magnetic field, suggesting the involvement of multiple carrier types in the transport mechanism. The coexistence of positive and negative slopes in Hall resistivity across varying temperatures underscores the predominance of electrons as the primary charge carriers. Furthermore, at 1 T, the Hall coefficient ($R_H$) exhibits a pronounced temperature dependence. The carrier concentration ($n$) and mobility ($\mu$) were quantitatively ascertained using eqn (1) and (2), respectively, based on the Hall resistivity data:[14]

$$n = \frac{1}{R_H \cdot e} \quad (1)$$

$$\mu = \frac{1}{e \cdot \rho_s \cdot n} \quad (2)$$

Employing the relationship that links charge carrier density ($n$) to the electron charge ($e$), resistivity ($\rho$), and the Hall coefficient (typically measured in units of $m^3\ C^{-1}$), both carrier concentration and mobility were calculated at various temperatures, as delineated in Table S1.† Our findings demonstrate

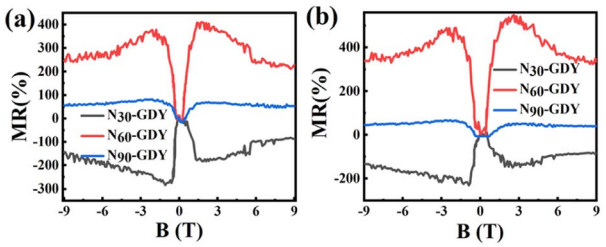


Fig. 5 (a) and (b) Depict the magnetoresistance of $N_{30}$-GDY, $N_{60}$-GDY, and $N_{90}$-GDY, measured at 2 K and 10 K, respectively.

that N-doping in GDY culminates in a substantial enhancement of carrier concentration, approximately by an order of magnitude. This indicates that N-doping significantly elevates the carrier concentration within GDY. Given that nitrogen atoms possess higher electronegativity compared to carbon atoms, N-doping introduces additional electrons into the GDY structure, thereby augmenting carrier concentration. This elevated carrier concentration facilitates enhanced electron transport within the material, ultimately influencing its magnetoresistance (MR) properties.

The MR effect, defined as $\mathrm{MR}(B) = \left[\frac{R(B)}{R(0)} - 1\right] \times 100\%$, quantifies the extent of change in electrical resistance in response to external magnetic fields. As depicted in Fig. 5, our measurements conducted at 2 K within a ±9 T magnetic field range reveal distinct behaviors in N-doped GDY samples. Specifically, $N_{30}$-GDY, characterized by a lower nitrogen concentration, exhibits negative magnetoresistance (NMR) at low temperatures, attaining an MR ratio of approximately 200%. This phenomenon occurs because N atoms, serving as scattering centers, are introduced into GDY, yet their concentration remains insufficient to fully alter the material's transport mechanism. Consequently, the MR characteristics of the $N_{30}$-GDY sample are predominantly governed by the Weak Localization (WL) effect.[25] In contrast, with increasing nitrogen concentration, $N_{60}$-GDY and $N_{90}$-GDY display positive magnetoresistance (PMR), with $N_{60}$-GDY exhibiting a particularly pronounced PMR effect, resulting in a resistance change exceeding 400%. These distinct MR signatures in N-doped GDY indicate a substantial transformation in transport properties due to nitrogen incorporation. The experimental results demonstrate that N-doping effectively modulates the MR characteristics of carbon materials. As N-doping levels escalate, magnetoresistance initially increases and subsequently diminishes. At lower N-doping levels, the enhanced carrier concentration intensifies electron scattering in the magnetic field, leading to elevated magnetoresistance. However, at excessively high N-doping levels, surplus nitrogen atoms may engender defects or impurity centers, thereby diminishing electron transport efficiency and ultimately reducing magnetoresistance.[26,27]

## Conclusion

We successfully synthesized nitrogen-doped GDY with varying degrees of doping ($N_{30}$-GDY, $N_{60}$-GDY, $N_{90}$-GDY) by meticulously modulating the annealing duration in an $NH_3$ atmosphere. Detailed examinations *via* SEM and XPS revealed a clear trend: prolonged annealing times augmented the prominence of the nitrogen peak, thereby confirming effective nitrogen doping. Hall resistivity measurements indicated a consistent increase in carrier concentration with enhanced nitrogen doping. Further investigation into the MR properties unveiled intriguing disparities among the doped samples. $N_{30}$-GDY exhibited NMR, indicative of weak localization effects, whereas $N_{60}$-GDY and $N_{90}$-GDY displayed PMR with significant resistance enhancements, signifying a transition in magneto-response behavior. We attribute these modifications primarily to the modulation of carrier concentration by nitrogen doping, which substantially impacted the MR properties. Our experiments provide valuable insights into the tuning of electronic and magnetic properties through chemical doping strategies, with significant implications for the development of advanced carbon-based electronic devices.

## Data availability

The data that support the fundings of this study are available from the corresponding author upon reasonable request.

## Conflicts of interest

There are no conflicts to declare.

## Acknowledgements

This research was funded by the Natural Science Foundations of Fujian Province (Grant No. 2024J01470, 2023J01350) and Dr Start Funding from Longyan University (LB2023009).

## References

1 G. X. Li, Y. L. Li, H. B. Liu, Y. B. Guo, Y. J. Li and D. B. Zhu, *Chem. Commun.*, 2010, **46**, 3256–3258.
2 J. Kang, J. B. Li, F. G. Wu, S. S. Li and J. B. Xia, *J. Phys. Chem. C*, 2011, **115**, 20466–20470.
3 S. W. Cranford and M. Buehler, Mechanical properties of graphyne, *Carbon*, 2011, **49**, 4111–4121.
4 Y. Y. Zhang, Q. X. Pei and C. M. Wang, *Appl. Phys. Lett.*, 2012, **101**, 081909.
5 S. G. Pari, A. Cuéllar and B. M. Wong, *J. Phys. Chem. C*, 2016, **120**, 18871–18877.
6 R. Pietrzak, *Fuel*, 2009, **88**, 1871–1877.
7 R. H. Baughman, H. Eckhardt and M. Kertesz, *J. Chem. Phys.*, 1987, **87**, 6687–6699.
8 N. Narita, S. Nagai, S. G. Suzuki and K. J. Nakao, *Phys. Rev. B:Condens. Matter Mater. Phys.*, 1998, **58**, 11009–11014.
9 H. J. Cui, X. L. Sheng, Q. B. Yan, Q. R. Zheng and G. Su, *Phys. Chem. Chem. Phys.*, 2013, **15**, 8179–8185.
10 M. Q. Long, L. Tang, D. Wang, Y. L. Li and Z. G. Shuai, *ACS Nano*, 2011, **5**, 2593–2600.
11 N. Wang, J. J. He, K. Wang, Y. J. Zhao, T. G. Jiu, C. S. Huang and Y. L. Li, *Adv. Mater.*, 2019, **31**, 1803202.

12 T. Wang and Z. L. Jin, *Results Surf. Interfac.*, 2024, **14**, 100188.
13 Y. P. Zheng, Y. H. Chen, L. H. Lin, Y. Y. Sun, H. B. Liu, Y. L. Li, Y. W. Du and N. J. Tang, *Appl. Phys. Lett.*, 2017, **111**, 033101.
14 M. Rein, N. Richter, K. Parvez, X. L. Feng, H. Sachdev, M. Kläui and K. Müllen, *ACS Nano*, 2015, **9**, 1360–1366.
15 H. F. Kang, B. C. Hua, L. Q. Xu, X. L. Zhan, Y. P. Zheng and Z. G. Huang, *Carbon*, 2021, **184**, 526–533.
16 H. Estrade-Szwarckopf, *Carbon*, 2004, **42**, 1713–1721.
17 F. Tuinstra and J. L. Koenig, *J. Chem. Phys.*, 1970, **53**, 1126–1130.
18 H. H. Bao, L. Wang, C. Li and J. Luo, *ACS Appl. Mater. Interfaces*, 2018, **11**, 2717–2729.
19 J. Li, X. Gao, B. Liu, Q. L. Feng, X. B. Li, M. Y. Huang, Z. F. Liu, J. Zhang, C. H. Tung and L. Z. Wu, *J. Am. Chem. Soc.*, 2016, **138**, 3954–3957.
20 P. Nowicki, R. Pietrzak and H. Wachowska, *Energy Fuels*, 2010, **24**, 1197–1206.
21 K. Ihm, T. H. Kang, D. H. Lee, S. Y. Park, K. J. Kim, B. Kim, J. H. Yang and C. Y. Park, *Surf. Sci.*, 2006, **600**, 3729–3733.
22 J. Liu, H. B. Liu, Y. L. Li, Y. P. Yi, X. K. Shang, S. S. Zhang, X. L. Yu, S. J. Zhang, H. B. Cao and G. J. Zhang, *Nanoscale*, 2014, **6**, 11336–11343.
23 R. Pietrzak, *Fuel*, 2009, **88**, 1871–1877.
24 A. Actis, P. D. Paolo Fornasiero, P. D. Mario Chiesa and P. D. Enrico Salvadori, *ChemPhotoChem*, 2024, **8**, e202300203.
25 I. V. Ovsienko, T. A. Len, L. Yu. Matsuy, Yu. I. Prylutskyy, I. B. Berkutov, V. V. Andrievskii, Yu. F. Komnik, I. G. Mirzoiev, G. E. Grechnev, Yu. A. Kolesnichenko, R. Hayn and P. Scharff, *Phys. Status Solidi B*, 2015, **252**, 1402–1409.
26 L. Lin, J. Y. Li, Q. H. Yuan, Q. H. Li, J. C. Zhang, L. Z. Sun, D. G. Rui, Z. L. Chen, K. C. Jia, M. Z. Wang, Y. F. Zhang, M. H. Rummeli, N. Kang, H. Q. Xu, F. Ding, H. L. Peng and Z. F. Liu, *Sci. Adv.*, 2019, **5**, eaaw8337.
27 F. Joucken, L. Henrard and J. Lagoute, *Phys. Rev. Mater.*, 2019, **3**, 110301.